Porosity Controls Spread of Excitation in Tectorial Membrane Traveling Waves

Jonathan B. Sellon,[†‡] Roozbeh Ghaffari,[‡] Shirin Farrahi,[‡§] Guy P. Richardson,[¶] and Dennis M. Freeman[†‡§*]
[†]Harvard-Massachusetts Institute of Technology Division of Health Sciences and Technology, Cambridge, Massachusetts; [‡]Research Laboratory of Electronics and [§]Department of Electrical Engineering and Computer Science, Massachusetts Institute of Technology, Cambridge, Massachusetts; and [¶]Sussex Neuroscience, School of Life Sciences, University of Sussex, Falmer, Brighton, United Kingdom

ABSTRACT Cochlear frequency selectivity plays a key role in our ability to understand speech, and is widely believed to be associated with cochlear amplification. However, genetic studies targeting the tectorial membrane (TM) have demonstrated both sharper and broader tuning with no obvious changes in hair bundle or somatic motility mechanisms. For example, cochlear tuning of *Tectb*$^{-/-}$ mice is significantly sharper than that of *Tecta*$^{Y1870C/+}$ mice, even though TM stiffnesses are similarly reduced relative to wild-type TMs. Here we show that differences in TM viscosity can account for these differences in tuning. In the basal cochlear turn, nanoscale pores of *Tecta*$^{Y1870C/+}$ TMs are significantly larger than those of *Tectb*$^{-/-}$ TMs. The larger pore size reduces shear viscosity (by ~70%), thereby reducing traveling wave speed and increasing spread of excitation. These results demonstrate the previously unrecognized importance of TM porosity in cochlear and neural tuning.

INTRODUCTION

The mammalian inner ear separates sounds by their frequency content, and loss of this separation impairs our ability to understand speech in noisy environments in ways that cannot generally be compensated with a hearing aid. Whereas this problem is well understood, its molecular origins are not. The development of genetic models of hearing disorders has provided unique opportunities to study cellular and molecular mechanisms that underlie the remarkable frequency selectivity of mammalian hearing (1–4). Of the ~400 mutants with hearing impairments developed to date (3), a surprising number affect genes that specifically target the tectorial membrane (TM) (5–15), an extracellular matrix that overlies hair cells. Although TM mutants display an enormous range of hearing deficits, the physical mechanisms underlying those deficits remain unclear.

For example, *Tecta*$^{Y1870C/+}$ and *Tectb*$^{-/-}$ mutations target α- and β-tectorin, respectively. Both of these tectorins are structural macromolecules that are thought to contribute to elastic properties of the TM (Fig. 1 *A*). Both *Tecta*$^{Y1870C/+}$ and *Tectb*$^{-/-}$ mutants have normal hair bundles and TM attachments. However, they exhibit distinctly different hearing phenotypes: *Tectb*$^{-/-}$ mice have sharpened basilar membrane (BM) tuning by a factor of 2–3 at mid to high frequencies (7), whereas *Tecta*$^{Y1870C/+}$ mice have normal BM tuning (Fig. 1 *B*) and even broader neural tuning (5). Although this difference in tuning is fundamental to our understanding of the distinctive properties of mammalian hearing, the mechanism is not known.

Previous studies have shown that TM shear stiffness is reduced in both *Tecta*$^{Y1870C/+}$ and *Tectb*$^{-/-}$ mutants by approximately a factor of 2 relative to wild-type mice (16,17). Because the stiffnesses of *Tecta*$^{Y1870C/+}$ and *Tectb*$^{-/-}$ TMs are similar, stiffness alone cannot account for the sharpened tuning observed in *Tectb*$^{-/-}$ mutants relative to *Tecta*$^{Y1870C/+}$ mutants. However, there are also differences in viscous loss. The viscous component of *Tecta*$^{Y1870C/+}$ TM shear impedance is approximately a factor-of-3 smaller than that of wild-types (16). In contrast, the shear viscosity of *Tectb*$^{-/-}$ TMs is similar to that of wild-types (17). Paradoxically, the larger viscosity in *Tectb*$^{-/-}$ TMs is associated with sharper tuning, which is the opposite of predictions from conventional models of viscous loss (18–27).

Here we investigate an alternative mechanism based on TM traveling waves (17,28–36). We show that the effect of loss in waves is characteristically different from the effect of loss in conventional cochlear models. Furthermore, these studies show that porosity plays a key role in determining loss, and thereby spread of excitation, in both normal and mutant TMs. Thus, TM porosity, and not stiffness, underlies the striking differences in *Tecta*$^{Y1870C/+}$ and *Tectb*$^{-/-}$ hearing.

MATERIALS AND METHODS

Isolated TM preparations

TM segments were excised from the cochleae of adult (15–30 g, 4–8 weeks old) *Tecta*$^{Y1870C/+}$ (strain B6129F1/J), *Tectb*$^{-/-}$ and wild-type mice (strain 129SvEv/C57BL6J) using a previously published surgical technique (37). Briefly, the bone surrounding the cochlea was gently chipped away, until the organ of Corti and TM were exposed. We used dark-field illumination to visualize the TM around the cochlear turns. Segments of TM that were

Submitted September 20, 2013, and accepted for publication February 6, 2014.

*Correspondence: freeman@mit.edu

Editor: James Keener.

0006-3495/14/03/1406/8 $2.00

http://dx.doi.org/10.1016/j.bpj.2014.02.012

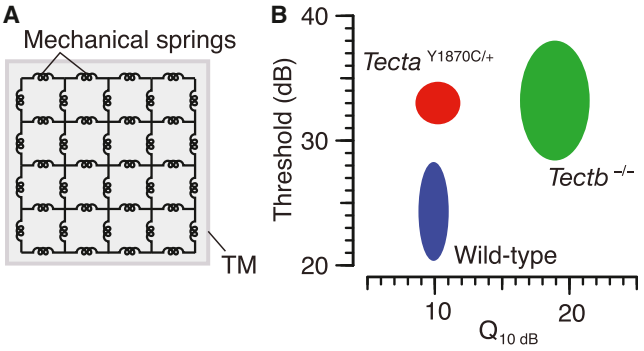

FIGURE 1 Model of TM material properties and measurements of sensitivity and frequency selectivity of TM mutant mice. (*A*) Schematic illustration of TM material properties, highlighting a network of mechanical springs that represent the stiffnesses of TM macromolecules. (*B*) BM threshold and quality of tuning measured (5,7) in the basal regions (50 kHz best frequency) of TM mutant mice: *Tecta*$^{Y1870C/+}$ (*red ellipse*, $n = 10$), *Tectb*$^{-/-}$ (*green ellipse*, $n = 8$), and wild-type (*blue ellipse*, $n = 24$).

0.5–1 mm in length were teased apart from the basal turn of the organ of Corti using a sterilized eyelash probe and then immersed in artificial endolymph (174 mM KCl, 5 mM HEPES, 3 mM dextrose, 2 mM NaCl, and 0.02 mM $CaCl_2$ titrated at pH 7.4). The care and use of animals in this study was approved by the Massachusetts Institute of Technology Committee on Animal Care.

Measuring TM wave properties

Isolated TM segments were suspended between vibrating and stationary supports in the wave chamber (17,28) (Fig. 2 *A*). The vibrating support was affixed with epoxy to a piezoelectric actuator (Thorlabs, Newton, NJ) and loosely coupled to the underlying glass slide, whereas the stationary support was firmly attached to the underlying glass slide. The surfaces of both supports were coated with 0.2 μL of tissue adhesive (Cel-Tak; Collaborative Research, Bedford, MA) and perfused with artificial endolymph. The TM was then injected into the bath and carefully attached to the surfaces of the supports in the regions coated with Cel-Tak (Collaborative Research). TM radial fibers were oriented in the direction parallel to the edge of the vibrating supports as shown in Fig. 2 *A* and *B*. TM shear viscosity was altered by adding PEG (polyethylene glycol; Sigma-Aldrich, St. Louis, MO) to artificial endolymph surrounding the TM in the wave chamber. To ensure adequate equilibration of PEG, the bath (5 mL) was exchanged four times over a time course of ~5 min. The final solution was allowed to equilibrate for 5 min before TM wave measurements were performed. Once measurements were completed, the bath was returned to normal artificial endolymph and wave measurements were repeated to test whether the response returned to initial conditions. This process was repeated for PEGs with a variety of molecular masses, and with concentrations chosen so that the viscosity of the bath was the same for each molecular mass (38):

1. 4 μM, 900 kDa;
2. 12 μM, 600 kDa;
3. 35 μM, 400 kDa;
4. 70 μM, 300 kDa;
5. 158 μM, 200 kDa;
6. 630 μM, 100 kDa; and
7. 15 mM, 8 kDa.

Viscosity was also altered by adding 9–11 kDa dextran (Sigma-Aldrich) to the artificial endolymph bath with a concentration (24 mM) chosen so that the viscosity (as measured with a kinematic viscometer (Technical Glass Products, Painesville, OH)) matched that of PEG solutions.

Optical imaging system

The optical imaging system consisted of a 20× water immersion objective (Zeiss Axioplan; Carl Zeiss, Oberkochen, Germany) with a 0.5 numerical aperture and a transmitted-light condenser (0.8 numerical aperture). Images were captured with an 8-megapixel charge-coupled device camera (Stingray; Allied Vision Technologies, Stadtroda, Germany). To capture motions at high frequencies, a stroboscopically pulsed light-emitting diode was synchronized to the audio frequency stimuli. To reconstruct wave motions, the TM was illuminated and images were captured at eight evenly spaced stimulus phases over several stimulus cycles. The collected images were then analyzed to determine the magnitude and phase of TM displacement at multiple regions along the TM's surface between the supports (39).

RESULTS

TM traveling waves in *Tecta*$^{Y1870C/+}$, *Tectb*$^{-/-}$, and wild-type mice

To characterize differences in *Tecta*$^{Y1870C/+}$ and *Tectb*$^{-/-}$ TMs, we measured wave motions (28) of isolated TMs from each of these mutants. TM segments were excised from the basal turn of the mouse cochlea and suspended between two supports immersed in artificial endolymph (Fig. 2 *A*). Forces were applied in the radial direction to these TM segments by driving one of the supports at audio frequencies (10–20 kHz). The amplitude and phase of TM radial displacements were measured at multiple points along the surface of the suspended TM using a previously published computer microvision technique (Materials and Methods). Complex exponentials were fit to the waveforms collected at eight phases to determine wavelength (λ; 2π divided by the slope of phase versus distance), speed (V; product of the wavelength and stimulus frequency), and decay constant (σ; distance the wave propagates before its amplitude decays by a factor of e).

Fig. 2 *B* shows snapshots of representative TM waves in response to 20 kHz stimuli from basal segments excised from wild-type, *Tecta*$^{Y1870C/+}$, and *Tectb*$^{-/-}$ mice. The frequency dependence of speed and decay for *Tecta*$^{Y1870C/+}$ ($n = 7$ preparations), *Tectb*$^{-/-}$ ($n = 4$ preparations), and wild-type ($n = 5$ preparations) TMs were then pooled across a range of audio frequencies (10–20 kHz) (Fig. 2, *C* and *D*). Wild-type TM segments exhibited the highest wave speeds over the measured frequency range, whereas *Tectb*$^{-/-}$ and *Tecta*$^{Y1870C/+}$ TM speeds were significantly lower by ~20 and ~40%, respectively.

Decay constants generally decreased with increasing frequency (Fig. 2 *D*). *Tecta*$^{Y1870C/+}$ and wild-type TMs had similar decay constants with ranges spanning 135–400 μm between 10 and 20 kHz. In contrast, decay constants for *Tectb*$^{-/-}$ TMs were significantly smaller (by as much as a factor of 2.25) than those of *Tecta*$^{Y1870C/+}$ or wild-type TMs, particularly at 15–20 kHz where the range of *Tectb*$^{-/-}$ decay constants spans 80–150 μm.

In summary, *Tecta*$^{Y1870C/+}$ and *Tectb*$^{-/-}$ mutations have different effects on TM wave speed and decay,

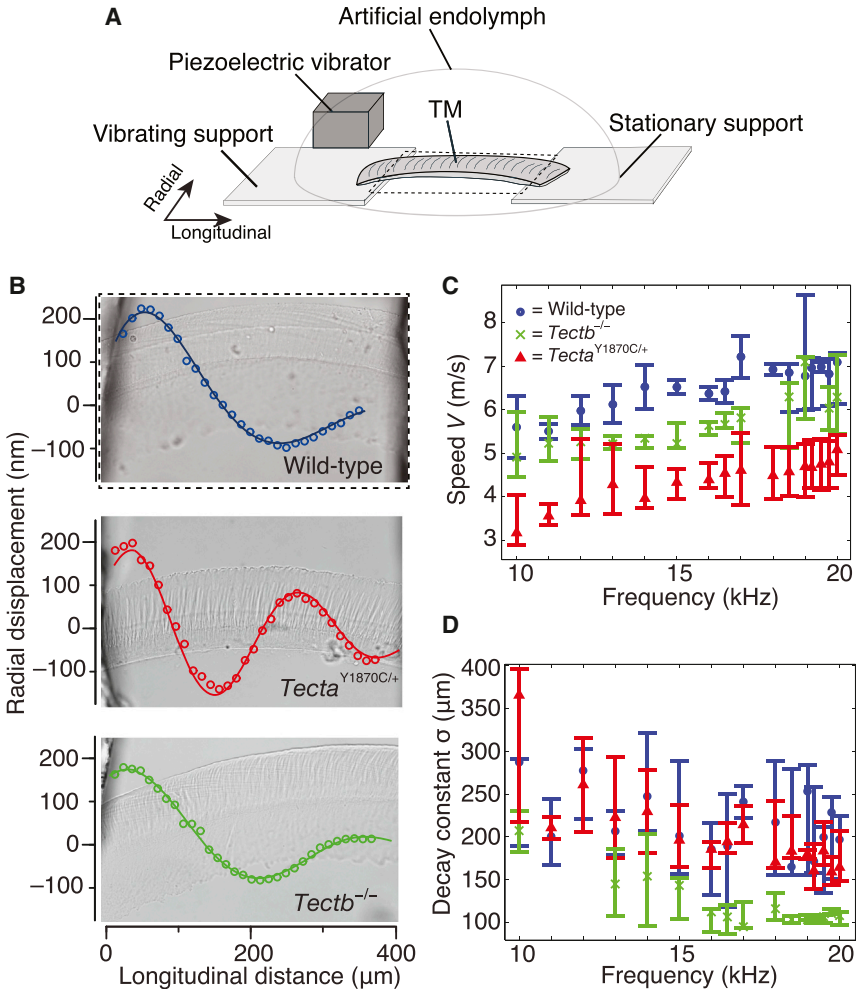

FIGURE 2 TM traveling waves in tectorin mutant and wild-type mice. (*A*) Schematic drawing of a wave chamber (28) showing TM segments suspended between vibrating and stationary supports (separated by ~200–400 μm) immersed in artificial endolymph. (*B*) Light microscope images of wild-type (*top*), *Tecta*$^{Y1870C/+}$ (*middle*), and *Tectb*$^{-/-}$ (*bottom*) TMs with representative wave motion snapshots (at 20 kHz) marked on the images. Nanometer-scale radial displacements are exaggerated by a factor of 600 for visualization. Lines through the data points denote best fits to the motion. Best-fitting wave parameter estimates were $\sigma = 161$ μm and $\lambda = 369$ μm (speed = 7.38 m/s) for this wild-type TM, $\sigma = 234$ μm and $\lambda = 228$ μm (speed = 4.56 m/s) for this *Tecta*$^{Y1870C/+}$ TM, and $\sigma = 111$ μm and $\lambda = 320$ μm (speed = 6.40 m/s) for this *Tectb*$^{-/-}$ TM. (*C*) Wave speed measurements pooled across multiple TM samples. Median TM wave speeds of *Tecta*$^{Y1870C/+}$ (*red triangles*) (n = 7 preparations), *Tectb*$^{-/-}$ (*green crosses*) ($n = 4$ preparations), and wild-types (*blue circles*) ($n = 5$ preparations) increased with stimulus frequency with differences across each mutant and wild-type. The range of speeds in *Tecta*$^{Y1870C/+}$ mutant TMs was significantly lower than those in wild-type and *Tectb*$^{-/-}$ TMs by up to 40%. (*Vertical bars*) Interquartile range (IQR) relative to the median speed. (*D*) Wave decay constant measurements pooled across multiple TM samples. *Tecta*$^{Y1870C/+}$ ($n = 7$ TM preparations; *red triangles*) and wild-type ($n = 5$ TM preparations; *blue circles*) had similar wave decay constants (σ) (135–325 μm for wild-types and 140–400 μm for *Tecta*$^{Y1870C/+}$ mutants), whereas *Tectb*$^{-/-}$ segments had significantly lower σ-estimates (80–225 μm).

$$V_{wt} > V_b > V_a$$

and

$$\sigma_{wt} \sim \sigma_a > \sigma_b,$$

where V and σ represent speed and decay constant, respectively; and *wt*, *a*, and *b* represent wild-type, *Tecta*$^{Y1870C/+}$, and *Tectb*$^{-/-}$ TMs, respectively.

TM material properties account for differences in wave properties

Wave properties of viscoelastic solids derive from material properties, including density (ρ), shear storage modulus (G'), and shear viscosity (η) (28,40). For infinite and isotropic materials, speed V and decay σ are expressed as

$$V = \sqrt{\frac{2(G'^2 + \omega^2\eta^2)}{\rho\left(\sqrt{G'^2 + \omega^2\eta^2} + G'\right)}}$$

and

$$\sigma = \sqrt{\frac{2(G'^2 + \omega^2\eta^2)}{\rho\omega^2\left(\sqrt{G'^2 + \omega^2\eta^2} - G'\right)}},$$

where ρ is density, and ω is the angular frequency ($\omega = 2\pi f$).

To account for boundary conditions in the wave chamber, we also developed a lumped model (Fig. 3 *A*), consisting of a distributed series of masses coupled by viscous and elastic elements (28). We used this model to determine the general relation between wave properties and material properties, which is illustrated by the contour lines in Fig. 3 *B*. We also used the model to compute the material properties that best fit each of the measured TM waves. The mean and standard deviation of the best fit parameters for *Tecta*$^{Y1870C/+}$, *Tectb*$^{-/-}$, and wild-type TMs stimulated from 17 to 20 kHz are included as colored ellipses in Fig. 3, *B* and *C*.

Estimates of shear storage modulus, G', are similar for *Tecta*$^{Y1870C/+}$ (23.8 $\pm$ 3.5 kPa; $n = 5$ TM preparations) and *Tectb*$^{-/-}$ (20.2 $\pm$ 8.1 kPa; $n = 4$ TM preparations) TMs, and both are significantly smaller than those of

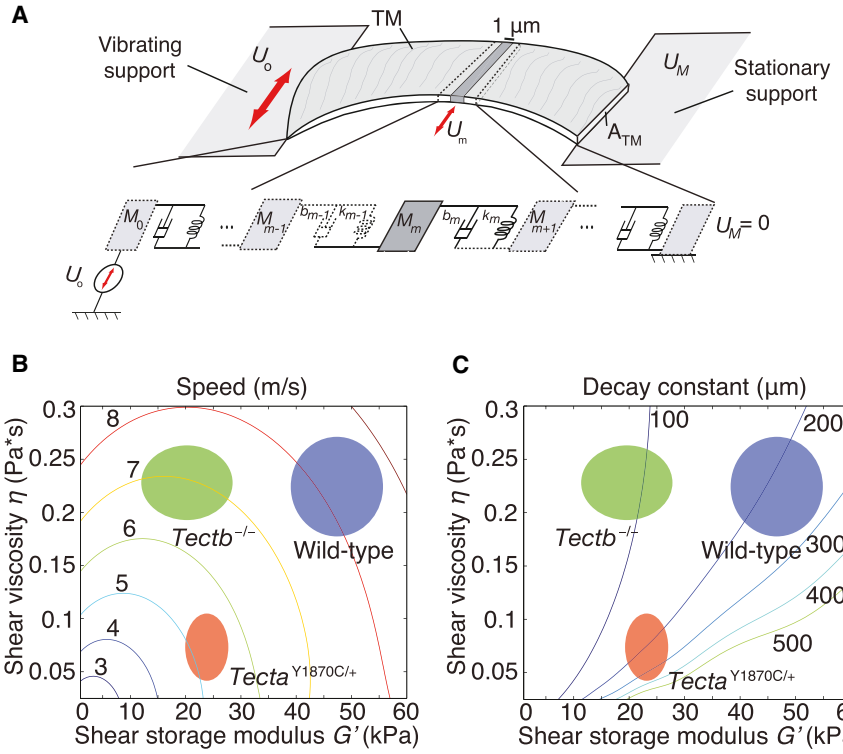

FIGURE 3 Distributed impedance model of the TM. (*A*) (*Upper*) Schematic drawing illustrating 1-μm longitudinal section of the TM (*dark gray*) with rectangular cross-sectional area, A_{TM}. The vibrating support was set to move with velocity, U_o, which in turn generated radial motion of TM sections, U_m, through longitudinal coupling. Motion was then terminated at the stationary support, where U_M was constrained to be zero. (*Lower*) Mechanical circuit representation of the TM consisting of a series of masses (M_m) coupled to adjacent sections by viscous (b_m) and elastic (k_m) components. (*B* and *C*) Contour plots show shear viscosity η and shear storage modulus G' parameter space at 20 kHz with lines denoting range of values for wave speed (*B*) and wave decay (*C*). (*Colored shaded ellipses* pasted on the contours) Ranges of G' and η estimates based on best fits to wave data in wild-types (*blue*), *Tecta*$^{Y1870C/+}$ (*red*), and *Tectb*$^{-/-}$ (*green*) TMs.

wild-types (47.7 $\pm$ 8.8 kPa; $n = 5$ TM preparations). Although G' is similar in *Tecta*$^{Y1870C/+}$ and *Tectb*$^{-/-}$ mutant TMs, there are significant differences in TM shear viscosity, η. *Tecta*$^{Y1870C/+}$ TMs have significantly lower η-values (0.073 $\pm$ 0.033 Pa·s; $n = 5$ TM preparations) compared to both *Tectb*$^{-/-}$ (0.23 $\pm$ 0.033 Pa·s; $n = 4$ TM preparations) and wild-type TMs (0.22 $\pm$ 0.048 Pa·s; $n = 5$ TM preparations), indicating that the key difference between *Tecta*$^{Y1870C/+}$ and *Tectb*$^{-/-}$ TMs is in their intrinsic shear viscosity.

In summary, the material properties of *Tecta*$^{Y1870C/+}$, *Tectb*$^{-/-}$, and wild-type TMs are different:

$$G'_{wt} > G'_b \sim G'_a$$

and

$$\eta_{wt} \sim \eta_b > \eta_a.$$

Whereas the stiffnesses of *Tecta*$^{Y1870C/+}$ and *Tectb*$^{-/-}$ TMs are similar, their shear viscosities are not. To understand the molecular mechanisms underlying the difference in shear viscosity, we must probe not only the viscoelastic properties (28,41–43) of the TM, but also the poroelastic properties.

Porosity is greater in *Tecta*$^{Y1870C/+}$ TMs than in *Tectb*$^{-/-}$ or wild-type TMs

The material properties of the TM are determined not only by the matrix of macromolecules, but also by their interactions with interstitial fluid. Forces of fluid origin depend on both the viscosity of the fluid and the distance between macromolecules, which can be characterized by an effective pore size. To characterize effects of viscosity we added PEG (molecular mass 8 kDa) to the artificial endolymph bath, so as to increase the viscosity by a factor of ~8.9. Wave speed increased ~37% and decay constants decreased ~47% (see Fig. S1 in the Supporting Material). To determine whether physicochemical effects other than viscosity contributed to these changes, we repeated the experiment with dextran (molecular mass 9–11 kDa) at the same viscosity. Wave speed increased ~42% and decay constants decreased ~46% (see Fig. S1). These results suggest that the primary effects of PEG and dextran can be attributed to viscosity.

To characterize the porous nature of the TM, we increased the viscosity of the artificial endolymph bath using PEGs with a range of molecular masses from 8 to 900 kDa, chosen to provide a range of radii of gyration (44). The relation between radius of gyration, R_g, and molecular weight, W, is given by Bhat and Timasheff (45) as

$$R_g = \left(\frac{3\eta W}{10\pi N\zeta^3}\right)^{\frac{1}{3}},$$

where N is the Avogadro number, ζ is the Flory-Fox parameter (taken as 0.8), and η is the intrinsic viscosity of the PEG solution, given by

$$\eta = 0.0646W^{0.645}.$$

The concentration of PEG used for each molecular weight was adjusted so that the viscosity of the bath was 8.9 times that of water (46). Fig. 4 *A* shows that adding large molecular weight PEGs had negligible effect on wave speed, but adding small molecular weight PEGs increased speeds by as much as 75%, suggesting that only PEGs that are small enough to permeate TM pores are able to alter the TM's internal shear viscosity and impact wave properties. Wave speeds increased by >15% when the molecular mass of the PEG was <500, 180, and 175 kDa for *Tecta*$^{Y1870C/+}$, *Tectb*$^{-/-}$, and wild-type TMs, respectively. Thus, the porosity of *Tecta*$^{Y1870C/+}$ TMs (~32–40 nm radii) is significantly greater than those of *Tectb*$^{-/-}$ and wild-type TMs (~15–22 nm radii) (Fig. 4 *B*).

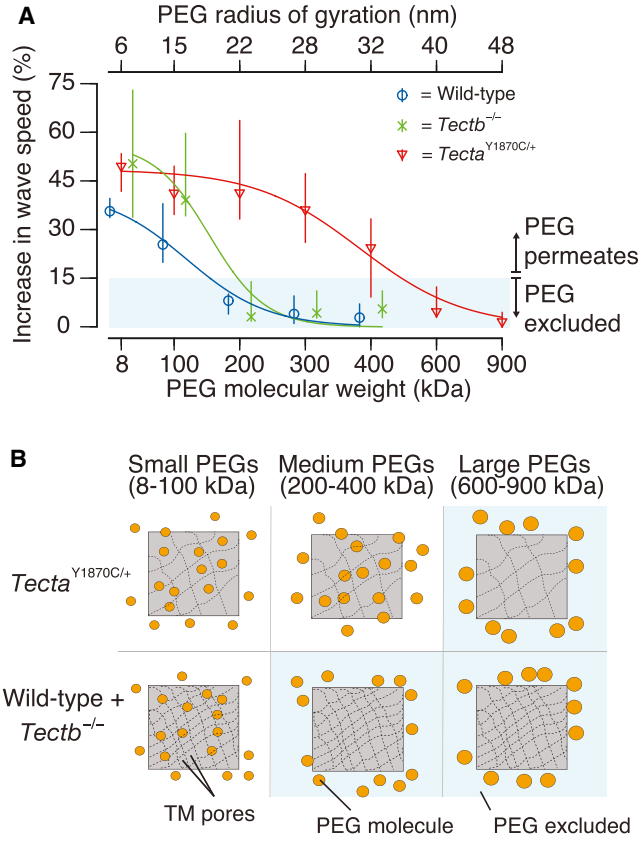

FIGURE 4 TM porosity in tectorin mutant and wild-type mice. (A) Polyethylene glycols (PEGs) with varying molecular masses (8–900 kDa) added to artificial endolymph surrounding *Tecta*$^{Y1870C/+}$, *Tectb*$^{-/-}$, and wild-type TMs, caused changes in wave speed at 10–20 kHz that correlate with increases in shear viscosity. The percent increase in wave speed caused by adding PEG is relative to measurements made in artificial endolymph. Large PEGs did not permeate the TM and had little effect on TM wave properties, whereas smaller PEGs that permeated the TM caused an increase in speed (above *shaded region*). PEGs with a radius of gyration <20 nm permeated wild-type TMs (*blue circles*, median and IQR; $n = 3$ TM preparations) and *Tectb*$^{-/-}$ mutant TMs (*green crosses*, median and IQR; $n = 3$ TM preparations) whereas PEGs with <36 nm radii permeated *Tecta*$^{Y1870C/+}$ mutant TMs (*red pluses*, median and IQR; $n = 4$ TM preparations). Medians were fit to sigmoid functions. For visual clarity, the median and IQR for wild-type and *Tectb*$^{-/-}$ mutant TMs were slightly offset relative to *Tecta*$^{Y1870C/+}$ median and IQR values at each PEG molecular weight reported on the *x* axis. (*B*) Schematic drawings of the TM highlighting its pores in the presence of small, medium, and large PEG molecules (*orange circles*). Small molecular weight PEGs (<36 nm for *Tecta*$^{Y1870C/+}$, < 20 nm for *Tectb*$^{-/-}$ and wild-types) are able to permeate the TM. In contrast, the *shaded-blue* examples show that some medium and all large PEG molecules are excluded from the TM depending on pore size; these *shaded regions* correlate with the findings in panel *A*.

These results suggest that the important difference between *Tecta*$^{Y1870C/+}$ and *Tectb*$^{-/-}$ TMs is their porosity. To directly test this hypothesis, we increased the viscosity of *Tecta*$^{Y1870C/+}$ TMs to match that of *Tectb*$^{-/-}$ TMs. Fig. 5 *A* and *B* shows that the addition of 5.5 mmol/L of 8 kDa PEG causes *Tecta*$^{Y1870C/+}$ TM waves to propagate with speeds and decays of *Tectb*$^{-/-}$ TMs across the range of measured frequencies, effectively transforming *Tecta*$^{Y1870C/+}$ TM wave behavior to mimic that of *Tectb*$^{-/-}$ TM waves.

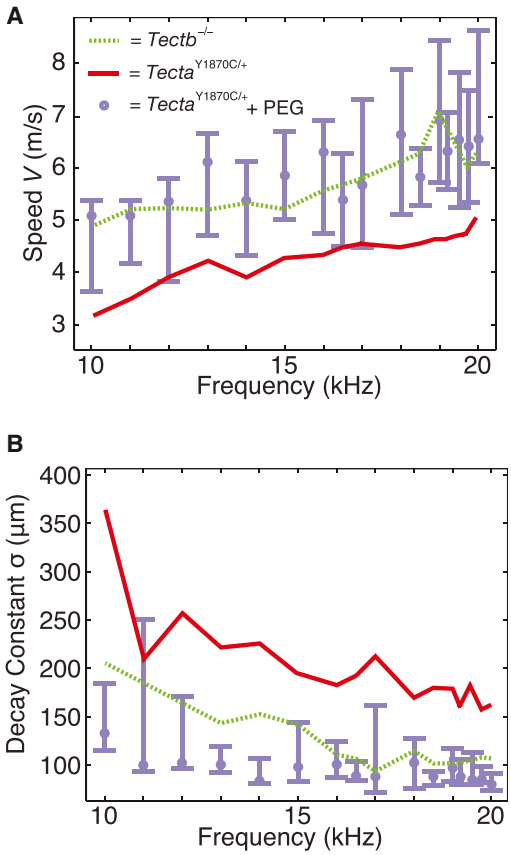

FIGURE 5 Frequency dependence of *Tecta*$^{Y1870C/+}$ TM wave speed and decay in high viscosity artificial endolymph. (*A*) Adding PEG to *Tecta*$^{Y1870C/+}$ TMs (*purple data*; $n = 4$ TM preparations) increased wave speeds relative to wave measurements taken before addition of PEG (*red line*, medians from Fig. 2 *C*), such that speeds match those of *Tectb*$^{-/-}$ TMs across all measured frequencies (*green dashed line*, median values from Fig. 2 *C*). (*B*) Adding PEG decreased *Tecta*$^{Y1870C/+}$ TM wave decay constants (*purple data*; $n = 4$ TM preparations) relative to wave measurements taken before administering PEG. Similar to panel *A*, these decay constants approached *Tectb*$^{-/-}$ TM decay median values. (*Solid circles* and *vertical lines*) Median values and IQR ranges, respectively, for panels *A* and *B*.

In summary, TM porosity generally plays an important role in determining wave properties, and more specifically, it is the critical parameter that determines the difference in the spread of excitation between *Tecta*$^{Y1870C/+}$ and *Tectb*$^{-/-}$ TMs.

DISCUSSION

Importance of TM shear viscosity

Previous measurements have established the importance of TM stiffness in cochlear mechanics (28,41–43,47–55). However, our results show that TM stiffness alone cannot explain the differences in hearing phenotypes of *Tecta*$^{Y1870C/+}$ and *Tectb*$^{-/-}$ mutant mice. In addition to stiffness, shear viscosity of the TM (caused by the interaction of water with TM macromolecules) plays a key role in determining TM wave properties. Although TM stiffness can be measured statically, TM shear viscosity requires a dynamic method (28,41–43). Our measurements at audio frequencies show that TM shear viscosity is significantly lower in *Tecta*$^{Y1870C/+}$ TMs than in *Tectb*$^{-/-}$ and wild-type TMs (Fig. 3 *B* and *C*). Reducing TM shear viscosity reduces wave transmission loss, which, in turn, allows TM waves in *Tecta*$^{Y1870C/+}$ mutants to propagate further than those in *Tectb*$^{-/-}$ mice (i.e., wave decay constants are larger in *Tecta*$^{Y1870C/+}$ mutants than in *Tectb*$^{-/-}$ mutants). These findings demonstrate that the TM is not a purely elastic structure, but rather, it has important viscoelastic properties that can help explain the differences in hearing phenotypes of *Tecta*$^{Y1870C/+}$ and *Tectb*$^{-/-}$ mutant mice.

TM porosity in tectorin mutants and wild-types

The smaller shear viscosity of *Tecta*$^{Y1870C/+}$ mutant TMs relative to *Tectb*$^{-/-}$ and wild-type TMs correlates with the larger pores measured in equilibrium osmotic measurements of *Tecta*$^{Y1870C/+}$ TMs (16). To test the relation between viscosity and porosity, we introduced PEG molecules with different radii of gyration in the bath surrounding the TM. We found a significant increase in internal shear viscosity only when the radius of gyration of PEG was sufficiently small to permeate the pores of the TM. The increase in internal shear viscosity induced by permeant PEG molecules alters both the speed and decay of TM waves. In particular, we show that by adding PEG to *Tecta*$^{Y1870C/+}$ TMs, we can transform their wave speeds and decay constants to match those of *Tectb*$^{-/-}$ TMs (Figs. 5 and 6 *A*). Therefore, differences in porosity alone account for differences in tuning between these mutants.

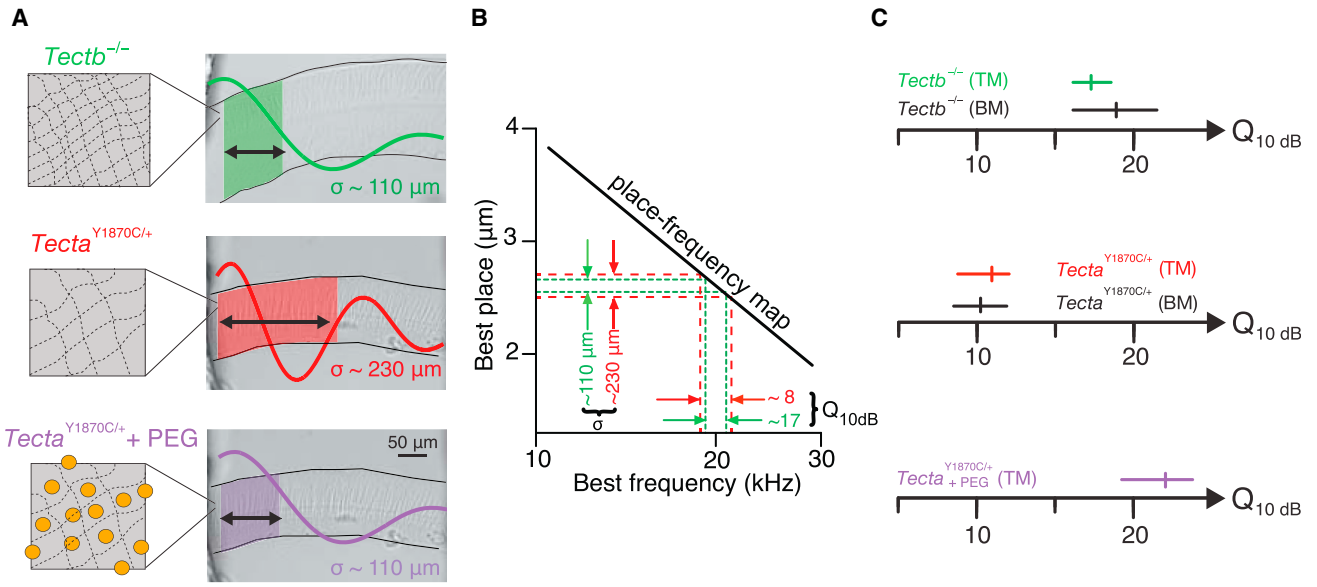

FIGURE 6 Relation between TM wave decay and quality of tuning. (*A*) Schematic drawings (*left*) and images (*right*) of *Tectb*$^{-/-}$ (*top*) and *Tecta*$^{Y1870C/+}$ (*middle*) TMs in artificial endolymph, and of a *Tecta*$^{Y1870C/+}$ TM perfused with PEG (*bottom*). (*Top* and *bottom black lines*) Marginal and limbal boundaries of the TMs, respectively. Waveforms superimposed on images illustrate TM waves in response to 20 kHz stimulation (*vertical scale* exaggerated for clarity). (*Shaded regions* with *double-sided arrows*) Spatial extent of TM waves with associated decay constants: σ = 110 μm for *Tectb*$^{-/-}$ (*green*); 230 μm for *Tecta*$^{Y1870C/+}$ (*red*); and 110 μm for *Tecta*$^{Y1870C/+}$+PEG (*purple*). (*B*) Relation between TM decay constants and frequency tuning. (*Solid black line*) Relation between best place and best frequency given by the cochlear map of the mouse (57). (*Horizontal dashed lines*) Separations with a decay constant for *Tectb*$^{-/-}$ (*green*, 110 μm) and *Tecta*$^{Y1870C/+}$ (*red*, 230 μm) TM samples. (*Vertical dashed lines*) Separations with an equivalent difference in frequency, from which Q_{10dB} can be calculated as ~8 for *Tecta*$^{Y1870C/+}$, and ~17 for *Tectb*$^{-/-}$. (*C*) Qualities of tuning (Q_{10dB}). *Tectb*$^{-/-}$ (*top*): Q_{10dB} calculated as shown in panel *B* for *Tectb*$^{-/-}$ TMs (median and interquartile range at 20 kHz) and compared to measurements of BM tuning (mean and standard deviation at 50 kHz, Russell et al. (7)). *Tecta*$^{Y1870C/+}$ (*middle*): Q_{10dB} calculated as shown in panel *B* for *Tecta*$^{Y1870C/+}$ TMs (median and interquartile range at 20 kHz) and compared to measurements of BM tuning (mean and standard deviation at 50 kHz, Legan et al. (5)). *Tecta*$^{Y1870C/+}$ TM perfused with PEG (*bottom*): Q_{10dB} increased by a factor of 2 relative to *Tecta*$^{Y1870C/+}$ TM measurements in normal artificial endolymph (without PEG).

Implications for cochlear and neural tuning

The effect of viscosity on TM waves and classical TM models is strikingly different. Classical models have suggested that viscous damping in the subtectorial space plays a critical role in determining frequency tuning and sensitivity in mammalian hearing (21–26). In particular, fluid viscosity limits sensitivity and sharpness of cochlear tuning. Our results suggest that viscous loss in the TM has the opposite effect on tuning. *Tecta*$^{Y1870C/+}$ TMs exhibit less loss (shear viscosity), which, in turn, increases the spatial extent of traveling waves relative to *Tectb*$^{-/-}$ mutants. When combined with scaling symmetry and the cochlear map of the mouse cochlea, this increase in spread of excitation would lead to broader tuning (Fig. 6). Thus, TM waves may compensate (at least in part) for the dissipative effects of fluid damping in the subtectorial space.

Osmotic effects on TM porosity

Changes in TM porosity may also be important in cochlear insults that induce physicochemical changes in endolymph. For instance, increasing sodium ion concentration in endolymph causes swelling of the TM (37,56), which would increase the effective pore radius. Larger TM pores would tend to reduce shear viscosity, which, based on our results, would increase the spatial extent of waves (Figs. 4 and 5) and broaden cochlear tuning (Fig. 6). In contrast, ionic manipulations that shrink the TM, such as increasing calcium concentration (57), would tend to reduce porosity, and thereby, result in reduced spatial extent and sharper cochlear tuning. Hearing disorders associated with Ménière's disease and/or cochlear hydrops may thus result, in part, from alterations in TM porosity caused by changes in inner ear fluids.

CONCLUSION

Although undetectable in quasi-static measurement techniques, shear viscosity is essential to determining the response of the TM to audio frequency stimuli. Because 96% of TM mass is water, it is hardly surprising that viscous properties of the TM are important. What is more surprising is that TM shear viscosity can change even if the viscosity of the interstitial fluid is constant. Shear viscosity depends not only on fluid viscosity but also on porosity, which is a measure of the effective distances between TM macromolecules. Furthermore, our results show that porosity plays a key role in determining the cochlear phenotypes of *Tecta*$^{Y1870C/+}$ and *Tectb*$^{-/-}$ mutants. Thus, porosity represents a fundamental material property of the TM, which, in combination with shear storage modulus, determines the speed and decay of TM waves, and thus contributes to the exquisite sensitivity and frequency selectivity of mammalian hearing.

SUPPORTING MATERIAL

One figure is available at http://www.biophysj.org/biophysj/supplemental/S0006-3495(14)00189-1.

This research was supported by National Institutes of Health grant No. R01-DC00238. J.B.S. was supported in part by the National Science Foundation Graduate Research Fellowship Program under grant No. 1122374. J.B.S. and S.F. were supported in part by a training grant from the National Institutes of Health to the Speech and Hearing Bioscience and Technology Program in the Harvard-MIT Division of Health Sciences and Technology. G.P.R. was supported by Wellcome Trust grant No. 087737.

REFERENCES

1. Fettiplace, R., and C. M. Hackney. 2006. The sensory and motor roles of auditory hair cells. *Nat. Rev. Neurosci.* 7:19–29.
2. Ashmore, J. 2008. Cochlear outer hair cell motility. *Physiol. Rev.* 88:173–210.
3. Kikkawa, Y., Y. Seki, …, H. Yonekawa. 2012. Advantages of a mouse model for human hearing impairment. *Exp. Anim.* 61:85–98.
4. Brown, S. D., R. E. Hardisty-Hughes, and P. Mburu. 2008. Quiet as a mouse: dissecting the molecular and genetic basis of hearing. *Nat. Rev. Genet.* 9:277–290.
5. Legan, P. K., V. A. Lukashkina, …, G. P. Richardson. 2005. A deafness mutation isolates a second role for the tectorial membrane in hearing. *Nat. Neurosci.* 8:1035–1042.
6. Legan, P. K., V. A. Lukashkina, …, G. P. Richardson. 2000. A targeted deletion in α-tectorin reveals that the tectorial membrane is required for the gain and timing of cochlear feedback. *Neuron.* 28:273–285.
7. Russell, I. J., P. K. Legan, …, G. P. Richardson. 2007. Sharpened cochlear tuning in a mouse with a genetically modified tectorial membrane. *Nat. Neurosci.* 10:215–223.
8. McGuirt, W. T., S. D. Prasad, …, R. J. Smith. 1999. Mutations in COL11A2 cause non-syndromic hearing loss (DFNA13). *Nat. Genet.* 23:413–419.
9. Suzuki, N., K. Asamura, …, S. Usami. 2005. Type IX collagen knockout mouse shows progressive hearing loss. *Neurosci. Res.* 51:293–298.
10. Richardson, G. P., J. B. de Monvel, and C. Petit. 2011. How the genetics of deafness illuminates auditory physiology. *Annu. Rev. Physiol.* 73: 311–334.
11. Xia, A., S. S. Gao, …, J. S. Oghalai. 2010. Deficient forward transduction and enhanced reverse transduction in the α-tectorin C1509G human hearing loss mutation. *Dis. Model. Mech.* 3:209–223.
12. Steel, K. P. 2000. A take on the tectorial membrane. *Nat. Genet.* 24:104.
13. Verhoeven, K., L. van Laer, …, G. van Camp. 1998. Mutations in the human α-tectorin gene cause autosomal dominant non-syndromic hearing impairment. *Nat. Genet.* 19:60–62.
14. Lukashkin, A. N., P. K. Legan, …, G. P. Richardson. 2012. A mouse model for human deafness DFNB22 reveals that hearing impairment is due to a loss of inner hair cell stimulation. *Proc. Natl. Acad. Sci. USA.* 109:19351–19356.
15. Zwaenepoel, I., M. Mustapha, …, C. Petit. 2002. Otoancorin, an inner ear protein restricted to the interface between the apical surface of sensory epithelia and their overlying acellular gels, is defective in autosomal recessive deafness DFNB22. *Proc. Natl. Acad. Sci. USA.* 99:6240–6245.
16. Masaki, K., R. Ghaffari, …, A. J. Aranyosi. 2010. Tectorial membrane material properties in *Tecta*$^{Y1870C/+}$ heterozygous mice. *Biophys. J.* 99:3274–3281.
17. Ghaffari, R., A. J. Aranyosi, …, D. M. Freeman. 2010. Tectorial membrane traveling waves underlie abnormal hearing in *Tectb* mutant mice. *Nat. Commun.* 1:96. http://dx.doi.org/10.1038/ncomms1094.

18. Davis, H. 1958. A mechano-electrical theory of cochlear action [Une théorie de l'action cochléaire mécano-électrique]. *Ann. Otol. Rhinol. Laryngol.* 67:789–801.
19. Dallos, P., M. C. Billone, …, S. Raynor. 1972. Cochlear inner and outer hair cells: functional differences. *Science.* 177:356–358.
20. Billone, M., and S. Raynor. 1973. Transmission of radial shear forces to cochlear hair cells. *J. Acoust. Soc. Am.* 54:1143–1156.
21. Neely, S. T., and D. O. Kim. 1983. An active cochlear model showing sharp tuning and high sensitivity. *Hear. Res.* 9:123–130.
22. Neely, S. T., and D. O. Kim. 1986. A model for active elements in cochlear biomechanics. *J. Acoust. Soc. Am.* 79:1472–1480.
23. Allen, J. B. 1980. Cochlear micromechanics—a physical model of transduction. *J. Acoust. Soc. Am.* 68:1660–1670.
24. Zwislocki, J. J. 1979. Tectorial membrane: a possible sharpening effect on the frequency analysis in the cochlea. *Acta Otolaryngol.* 87: 267–269.
25. Zwislocki, J. J. 1980. Five decades of research on cochlear mechanics. *J. Acoust. Soc. Am.* 67:1679–1685.
26. Mammano, F., and R. Nobili. 1993. Biophysics of the cochlea: linear approximation. *J. Acoust. Soc. Am.* 93:3320–3332.
27. Gold, T. 1948. Hearing. II. the physical basis of the action of the cochlea. *Proc. R. Soc. Lond. B Biol. Sci.* 135:492–498.
28. Ghaffari, R., A. J. Aranyosi, and D. M. Freeman. 2007. Longitudinally propagating traveling waves of the mammalian tectorial membrane. *Proc. Natl. Acad. Sci. USA.* 104:16510–16515.
29. Richardson, G. P., A. N. Lukashkin, and I. J. Russell. 2008. The tectorial membrane: one slice of a complex cochlear sandwich. *Curr. Opin. Otolaryngol. Head Neck Surg.* 16:458–464.
30. Guinan, Jr., J. J., and N. P. Cooper. 2008. Medial olivocochlear efferent inhibition of basilar-membrane responses to clicks: evidence for two modes of cochlear mechanical excitation. *J. Acoust. Soc. Am.* 124: 1080–1092.
31. Meaud, J., and K. Grosh. 2010. The effect of tectorial membrane and basilar membrane longitudinal coupling in cochlear mechanics. *J. Acoust. Soc. Am.* 127:1411–1421.
32. Bergevin, C., and C. A. Shera. 2010. Coherent reflection without traveling waves: on the origin of long-latency otoacoustic emissions in lizards. *J. Acoust. Soc. Am.* 127:2398–2409.
33. Lukashkin, A. N., G. P. Richardson, and I. J. Russell. 2010. Multiple roles for the tectorial membrane in the active cochlea. *Hear. Res.* 266:26–35.
34. Jones, G. P., V. A. Lukashkina, …, A. N. Lukashkin. 2013. Frequency-dependent properties of the tectorial membrane facilitate energy transmission and amplification in the cochlea. *Biophys. J.* 104:1357–1366.
35. Hubbard, A. E. 1993. A traveling-wave amplifier model of the cochlea. *Science.* 259:68–71.
36. Lamb, J. S., and R. S. Chadwick. 2011. Dual traveling waves in an inner ear model with two degrees of freedom. *Phys. Rev. Lett.* 107: 088101.
37. Shah, D. M., D. M. Freeman, and T. F. Weiss. 1995. The osmotic response of the isolated, unfixed mouse tectorial membrane to isoosmotic solutions: effect of Na^{+}, K^{+}, and Ca^{2+} concentration. *Hear. Res.* 87:187–207.
38. Bailey, F., and R. Callard. 1959. Some properties of poly (ethylene oxide)1 in aqueous solution. *J. Appl. Polym. Sci.* 1:56–62.
39. Davis, C. Q., and D. M. Freeman. 1998. Using a light microscope to measure motions with nanometer accuracy. *Opt. Eng.* 37:1299–1304.
40. Greenleaf, J. F., M. Fatemi, and M. Insana. 2003. Selected methods for imaging elastic properties of biological tissues. *Annu. Rev. Biomed. Eng.* 5:57–78.
41. Abnet, C. C., and D. M. Freeman. 2000. Deformations of the isolated mouse tectorial membrane produced by oscillatory forces. *Hear. Res.* 144:29–46.
42. Gu, J. W., W. Hemmert, …, A. J. Aranyosi. 2008. Frequency-dependent shear impedance of the tectorial membrane. *Biophys. J.* 95:2529–2538.
43. Gavara, N., and R. S. Chadwick. 2010. Noncontact microrheology at acoustic frequencies using frequency-modulated atomic force microscopy. *Nat. Methods.* 7:650–654.
44. Masaki, K., T. F. Weiss, and D. M. Freeman. 2006. Poroelastic bulk properties of the tectorial membrane measured with osmotic stress. *Biophys. J.* 91:2356–2370.
45. Bhat, R., and S. N. Timasheff. 1992. Steric exclusion is the principal source of the preferential hydration of proteins in the presence of polyethylene glycols. *Protein Sci.* 1:1133–1143.
46. Gonzalez-Tello, P., F. Camacho, and G. Blazquez. 1994. Density and viscosity of concentrated aqueous solutions of polyethylene glycol. *J. Chem. Eng. Data.* 39:611–614.
47. Zwislocki, J. J., and L. K. Cefaratti. 1989. Tectorial membrane. II: Stiffness measurements in vivo. *Hear. Res.* 42:211–227.
48. Gueta, R., J. Levitt, …, I. Rousso. 2011. Structural and mechanical analysis of tectorial membrane Tecta mutants. *Biophys. J.* 100:2530–2538.
49. Gueta, R., E. Tal, …, I. Rousso. 2007. The 3D structure of the tectorial membrane determined by second-harmonic imaging microscopy. *J. Struct. Biol.* 159:103–110.
50. Gueta, R., D. Barlam, …, I. Rousso. 2006. Measurement of the mechanical properties of isolated tectorial membrane using atomic force microscopy. *Proc. Natl. Acad. Sci. USA.* 103:14790–14795.
51. Richter, C.-P., G. Emadi, …, P. Dallos. 2007. Tectorial membrane stiffness gradients. *Biophys. J.* 93:2265–2276.
52. Shoelson, B., E. K. Dimitriadis, …, R. S. Chadwick. 2004. Evidence and implications of inhomogeneity in tectorial membrane elasticity. *Biophys. J.* 87:2768–2777.
53. Freeman, D. M., C. C. Abnet, …, T. F. Weiss. 2003. Dynamic material properties of the tectorial membrane: a summary. *Hear. Res.* 180:1–10.
54. Gavara, N., D. Manoussaki, and R. S. Chadwick. 2011. Auditory mechanics of the tectorial membrane and the cochlear spiral. *Curr. Opin. Otolaryngol. Head Neck Surg.* 19:382–387.
55. Gavara, N., and R. S. Chadwick. 2009. Collagen-based mechanical anisotropy of the tectorial membrane: implications for inter-row coupling of outer hair cell bundles. *PLoS ONE.* 4:e4877.
56. Freeman, D. M., K. Masaki, …, T. F. Weiss. 2003. Static material properties of the tectorial membrane: a summary. *Hear. Res.* 180:11–27.
57. Müller, M., K. von Hünerbein, …, J. W. Smolders. 2005. A physiological place-frequency map of the cochlea in the CBA/J mouse. *Hear. Res.* 202:63–73.